BIOCHEMISTRY
including biophysical chemistry & molecular biology

Article

pubs.acs.org/biochemistry

Imaging of Protein Crystals with Two-Photon Microscopy

Pius Padayatti,[†] Grazyna Palczewska,[†] Wenyu Sun,[†] Krzysztof Palczewski,*[,‡] and David Salom[†]

[†]Polgenix Inc., Cleveland, Ohio 44106, United States

[‡]Department of Pharmacology, School of Medicine, Case Western Reserve University, 10900 Euclid Avenue, Cleveland, Ohio 44106, United States

Supporting Information

ABSTRACT: Second-order nonlinear optical imaging of chiral crystals (SONICC), which portrays second-harmonic generation (SHG) by noncentrosymmetric crystals, is emerging as a powerful imaging technique for protein crystals in media opaque to visible light because of its high signal-to-noise ratio. Here we report the incorporation of both SONICC and two-photon excited fluorescence (TPEF) into one imaging system that allows visualization of crystals as small as ~10 μm in their longest dimension. Using this system, we then documented an inverse correlation between the level of symmetry in examined crystals and the intensity of their SHG. Moreover, because of blue-green TPEF exhibited by most tested protein crystals, we also could identify and image SHG-silent protein crystals. Our experimental data suggest that the TPEF in protein crystals is mainly caused by the oxidation of tryptophan residues. Additionally, we found that unspecific fluorescent dyes are able to bind to lysozyme crystals and enhance their detection by TPEF. We finally confirmed that the observed fluorescence was generated by a two-photon rather than a three-photon process. The capability for imaging small protein crystals in turbid or opaque media with nondamaging infrared light in a single system makes the combination of SHG and intrinsic visible TPEF a powerful tool for nondestructive protein crystal identification and characterization during crystallization trials.

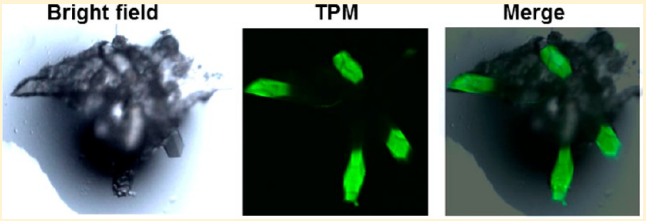

Reliable, accurate detection of protein microcrystals (cross sections of <100 μm^2) in crystallization media has become a high priority for collecting diffraction data for difficult protein targets. Recent success in obtaining data sets from small G protein-coupled receptor crystals (5−10 μm)[1,2] and the ability to collect data from third-generation X-ray beamlines equipped with microfocus/minibeam capabilities have demonstrated the feasibility of obtaining crystal structures of such difficult targets.[3] Membrane protein crystallization is often performed in highly viscous, nonuniform mesophase or lipid/detergent media, but the development of imaging techniques capable of identifying microcrystals against opaque and nonuniform backgrounds is highly challenging. This problem is underscored by the fact that the optically transparent mesophase formed by combining monoolein with protein/detergent micelles when mixed with various precipitants can become highly birefringent under bright field microscopes equipped with crossed polarizers, thereby complicating identification of crystals via their birefringence. Such practical difficulties demand the development of techniques that can be used to image the initial formation of microcrystals in membrane protein crystallization media.[4]

Much progress has been made over the past few years in developing imaging methods that help identify protein microcrystals. Among these, UV fluorescence elicited from native aromatic residues is the best studied.[5,6] More recent advances involve the use of UV transparent crystallization vessels and longer excitation wavelengths to reduce UV absorption by routinely used plastic plates.[7] Despite these improvements, UV detection methods remain unattractive because they can damage precious samples by harmful radiation and lack efficiency in microcrystal detection.[4] Another technique known as second-order nonlinear optical (NLO) imaging of chiral crystals (SONICC) has helped to solve many problems that previous techniques could not overcome.[8] The major advantages of SONICC are its higher signal-to-noise ratio and applicability to crystal detection in membrane protein crystallization media that employs lipidic cubic phases.[4] These studies highlighted a possible application of SHG in distinguishing protein crystals from inorganic and small molecule crystals.[8] Recently, two-photon excited UV fluorescence microscopy was used to generate images of protein crystals,[9] but the use of TPEF in the visible range has been limited to crystals of green fluorescent protein.[8]

SHG is a second-order NLO process in which two photons interact with a nonlinear material nearly simultaneously and, as a result, form a new photon with an energy equal to the sum of the incident photon energies and, thus, twice the frequency of the initial photons.[10] Similar to TPEF, the SHG signal is proportional to the square of the instantaneous excitation power and inversely proportional to the duration of the laser pulse. Whereas both TPEF and SHG are dipolar processes,

Received: November 8, 2011
Revised: February 10, 2012
Published: February 11, 2012

   dx.doi.org/10.1021/bi201682q | *Biochemistry* 2012, 51, 1625−1637

only SHG is a coherent process, with wave cancellation that occurs for signals generated from oppositely oriented structures. Thus, noncentrosymmetric crystallographic configurations are required for generation of second-harmonic signals. SHG has also emerged as a new contrast technique for identifying structurally ordered proteins such as collagen, myosin, and tubulin in their native tissues.[11−13] The same principle is expected to produce SHG from other biological structural materials such as protein crystals.

In our nonlinear imaging experiments, we confirmed earlier work demonstrating that this technique could detect microcrystals in mesophase crystallization trials[4] but also observed limitations in the use of SONICC. Specifically, protein crystals belonging to higher-symmetry crystallographic lattices lacked a detectable SHG signal. Moreover, we also observed that SHG arose from crystals of both chiral and achiral small molecules. To address these limitations of SONICC, we combined SHG with visible TPEF imaging, which then allowed protein crystals with higher symmetry to be readily observed. Moreover, we found that the oxidation of tryptophan residues may be responsible for the TPEF exhibited by most tested protein crystals.

EXPERIMENTAL PROCEDURES

Protein Preparations. All proteins used in this study were either purified in our laboratory or purchased in purified form. Bacteriorhodopsin, photosynthetic reaction center (RC), serotonin receptor type 4 (5-HT4R), rhodopsin, and RPE65 were prepared in house. Lysozyme (from hen egg white), endo-1,4-β-D-xylanase II (from *Trichoderma* sp.), and glucose isomerase (from *Streptomyces rubiginosus*) were purchased from Hampton Research (Aliso Viejo, CA); glucose isomerase was obtained as crystallites and dialyzed extensively against 10 mM HEPES (pH 7.0) before being crystallized. Lyophilized powders of thaumatin (*Thaumatococcus daniellii*) and ribonuclease A (RNase A) were purchased from Sigma (St. Louis, MO).

Bacteriorhodopsin was purified from purple membranes prepared from *Halobacterium salinarum* (ATCC 29341) by following an established purification protocol.[14] RC was purified from *Blastochloris viridis* (ATCC 19567) based on previously reported protocols with minor modifications.[15,16] Briefly, RC present in the solubilized membrane fraction was isolated by using diethylaminoethyl (DEAE)-cellulose anion exchange chromatography followed by gel filtration chromatography. 5-HT4R was expressed and immunopurified from transfected *Sf*9 insect cells according to methods outlined for mouse retina expressed receptor in ref 17. The sample was 95% pure as judged by sodium dodecyl sulfate−polyacrylamide gel electrophoresis and silver staining. RPE65 was purified from bovine RPE as reported in ref 18. Bovine rhodopsin was isolated from dark-adapted bovine retinas as described in ref 19.

Crystallization of Membrane Proteins. Membrane protein crystallization in a mesophase was performed as reported in ref 20. Bacteriorhodopsin was prepared for crystallization trials in a mesophase as described by Misquitta and Caffrey.[21] The bacteriorhodopsin sample was stripped of excess detergent [*n*-octyl β-D-glucopyranoside (Affymetrix, Santa Clara, CA)] in a batch process by using Extracti-Gel D detergent removal resin (Thermo Fisher Scientific, Rockford, IL). The resulting purified protein was mixed with molten monoolein (Nucheck Prep) at a ratio of 2:3 (w/w) in a syringe coupler (Emerald Biosystems, Bainbridge Island, WA) to obtain a clear mesophase that then was manually dispensed into 27-well slides (Saunders Corp.). We found that removal of excess detergent allowed overnight crystallization in mesophase trials. RC crystallization was performed in a mesophase as reported previously[15,16] with the following modifications. The protein was purified by gel filtration chromatography, concentrated to 18 mg/mL,[22] and supplemented with 3% (w/v) 1,2,3-heptanetriol, 20 mM NaH_2PO_4, 0.063% (w/v) lauryldimethylamine oxide (LDAO), and 1.5 M $(NH_4)_2SO_4$, to yield a final concentration of 11.25 mg/mL The resulting solution was mixed with monoolein and set up for crystallization in sandwich plates overlaid with 1.8−2.1 M $(NH_4)_2SO_4$. Hexagonal RPE65 crystals were grown as reported previously by our laboratory.[18] Orthorhombic RPE65 crystals were produced under similar crystallization conditions. Trigonal crystals of ground-state rhodopsin were grown as reported previously.[19,23] Rhodopsin crystals were imaged first with two-photon microscopy (TPM) in the dark and then photoactivated with white light for 2 min that changed their color from red to yellow,[19,23] after which they were imaged again. By repeating the emission spectrum scan, we estimated that ∼5% of rhodopsin was photoactivated during the scan of ground-state rhodopsin crystals with an excitation wavelength set to 910 nm.

Crystallization of Soluble Proteins. Glucose isomerase (15 mg/mL) and endo-1,4-β-D-xylanase II (10 mg/mL) crystals were obtained from the AmSO4 Suite (Qiagen, Valencia, CA). Glucose isomerase crystals were grown from a 1:1 (v/v) mixture of 15 mg/mL protein in water with a reservoir solution containing 2.2 M ammonium sulfate and 0.2 M sodium thiocyanate.[24] Endo-1,4-β-D-xylanase II crystals were grown in 1:1 (v/v) mixtures of 30 mg/mL protein in water and a well solution containing 1.6 M ammonium sulfate, 0.1 M HEPES (pH 7.5), and 0.2 M sodium chloride. Tetragonal lysozyme crystals were obtained from 1:1 (v/v) mixtures of ∼50 mg/mL lysozyme in 20 mM sodium acetate (pH 4.5) and a well solution containing 0.1 M sodium acetate (pH 4.5) and 0.8 M NaCl.[25] Triclinic lysozyme crystals were procured from a 1:1 (v/v) mixture of ∼50 mg/mL lysozyme and a well solution containing 0.1 M sodium acetate (pH 4.5) with 12% ethylene glycol and 0.3 M sodium nitrate.[26] Thaumatin was dissolved in water at 50 mg/mL and mixed in a 1:1 (v/v) ratio with a well solution containing 23−30% (w/v) sodium potassium tartrate, 15% (v/v) ethylene glycol, and 0.1 M Bis-Tris propane (pH 6.6).[27] RNase A was crystallized by mixing a 1:1 (v/v) mixture of 10 mg/mL protein with a well solution containing 0.05 M sodium citrate (pH 5.6) and 25% polyethylene glycol 4000.[28]

Nonprotein crystals were grown by vapor equilibration of a concentrated water solution against a saturated suspension of the same molecule. Crystals of 5-fluoro-2-methoxy(1-{2-[(methylsulfonyl)amino]ethyl}-4-piperidinyl)-1*H*-indole-3-methylcarboxylate sulfamate (GR125487) (Tocris, Ellisville, MO) were also grown by vapor diffusion during 5-HT4R crystallization trials, and their identity was confirmed by structural determination.

X-ray Diffraction and Space Group Determinations. Diffraction data were collected for most of the soluble proteins by using an in-house Rigaku (The Woodlands, TX) diffractometer. The space group assignment was confirmed by structural refinement. Crystals grown in a mesophase were screened at the Advanced Photon Source (APS, Chicago, IL) GM/CA-CAT 23-ID-B and NE-CAT 24-ID-C beamlines equipped with minibeam/microfocus capability for raster scanning diffraction properties of samples to locate micro-

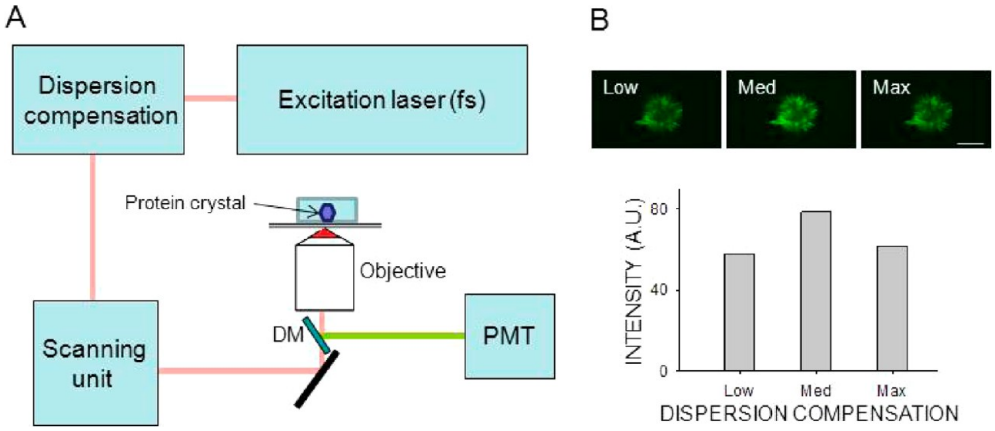

Figure 1. Detection of crystals by nonlinear imaging. Nonlinear images were obtained with a Leica TCS SP2 in an epi configuration equipped with galvanometer-driven scanners. (A) Diagram of the system. Infrared light from a tunable pulsed femtosecond laser was precompensated to minimize the impact of system dispersion. Incident light was focused on the sample with a high-NA objective. The nonlinear signal from the sample was collected by PMT without descanning, after separation of excitation light by a dichroic mirror (DM). (B) Two-photon excitation images (top) of protein crystals in a mesophase obtained at three different dispersion compensation settings. The scale bar is 150 μm. Nonlinear signal intensity (bottom) shown as a function of dispersion compensation. The optimal dispersion compensation setting increased the signal by 36%.

crystals within the frozen mesophase. Additional diffraction experiments were performed at NSLS beamline X29 (Brookhaven National Laboratory, Upton, NY) and at beamlines X06SA and X10SA of the Swiss Light Source (Paul Scherrer Institute, Villigen, Switzerland).

Setup for Nonlinear Imaging of Crystals. The experimental setup for SONICC/TPEF imaging in an epi configuration is shown in Figure 1. Both epi imaging and transmission nonlinear imaging were conducted with a Leica (Wetzlar, Germany) TCS SP2 confocal microscope equipped with a Chameleon XR tunable Ti:Sapphire laser (Coherent, Santa Clara, CA). To maximize the nonlinear signal, 90 MHz, 150 fs laser pulses were modulated by Chameleon PreComp with automated dispersion compensation. The laser beam was focused on the sample with either a 0.4 or 0.7 numerical aperture (NA) objective. For epi imaging, light emanating from the crystal was collected through the same lens, and a dichroic mirror was used to remove scattered excitation light and direct emitted light to a Hamamatsu (Shizuoka, Japan) R6357 photomultiplier tube (PMT) in a non-descanned configuration. The same type of detector was used for both epi and transmission imaging. For imaging in the transmission mode, the excitation light was directed to the PMT through a 425/50 m-2P bandpass filter (Chroma, Bellows Falls, VT), after being collected by a condenser lens with a 0.9 NA. To obtain high-signal-to-noise images with both TPEF and SHG, we had to maximize the laser pulse peak power. To accomplish this in addition to using a pulsed titanium−sapphire laser, we incorporated a dispersion compensation system that provided negative group velocity dispersion (GVD) to minimize pulse temporal broadening resulting from positive GVD introduced by the optics of the microscope. Spectral data were obtained without dichroic mirrors by using the built-in Leica TCS SP2 spectrally sensitive detector in a descanned configuration. The laser power in the sample plane was measured with a calibrated Coherent FieldMax-To laser power meter and a PM10 sensor. Signal intensities reflecting pixel values derived from raw images of regions outlined to contain a crystal were analyzed off-line by using Leica LCS Lite 2.6 and Sigma Plot 11.0 (Systat Software, Inc., San Jose, CA).

Crystals grown in a mesophase were imaged directly in a glass sandwich setup, with the coverslip facing the microscope objective. Crystals grown by vapor diffusion were transferred to an ~5 μL drop of reservoir solution placed in a glass-bottom 35 mm dish (MatTek Corp.) that also contained ~0.5 mL of reservoir solution, and the plate was kept sealed with vacuum grease during the experiment. In some experiments, <1 μL of a concentrated stock of ammonium persulfate (APS) or fluorescent dye, 4′,6-diamidino-2-phenylindole, dilactate (DAPI) (Life Technologies Corp., Carlsbad, CA), fluorescein (Polysciences Inc., Warrington, PA), or 1-hexanoyl-2-{6-[(7-nitro-2-1,3-benzoxadiazol-4-yl)amino]hexanoyl}-*sn*-glycero-3-phosphocholine (NBD PC) (Avanti Polar Lipids Inc., Alabaster, AL), was added to the drop containing the crystal to be imaged. Also in some cases, crystals were transferred instead to a drop of mineral oil that usually stabilized their integrity without affecting their spectral characteristics. For transmission mode imaging, crystals were placed between the two coverslips, separated by a spacer to avoid crystal damage and maintain an optimal working distance. Imaging was performed on multiple crystals for each crystal form even though, in most cases, only one representative image and emission scan is shown in the Results. Unless otherwise stated, imaging was performed with 730 or 850 nm incident light, and emission spectra were collected from 390 to 690 nm.

Spectrophotometry and One-Photon Spectrofluorimetry. Absorbance spectra were measured either with a 1 cm length path quartz cuvette in a Cary 50 Bio UV−vis spectrophotometer (Varian Inc., Walnut Creek, CA) or directly in a NanoDrop 1000 spectrophotometer (Thermo Scientific, Wilmington, DE) for 1 mm path length measurements. Fluorescence spectra were obtained from samples in a 1 cm × 1 cm quartz cuvette with an LS5 luminescence spectrophotometer (Perkin-Elmer, Walthman, MA) after excitation and emission wavelengths had been set to 365 and 485 nm, respectively, and both slits at 10 nm.

RESULTS

Two-Photon Microscopy. The experimental setup shown in Figure 1 was used to obtain TPM images of crystals based on both nonlinear processes, TPEF and SHG, unless otherwise

dx.doi.org/10.1021/bi201682q | *Biochemistry* 2012, 51, 1625−1637

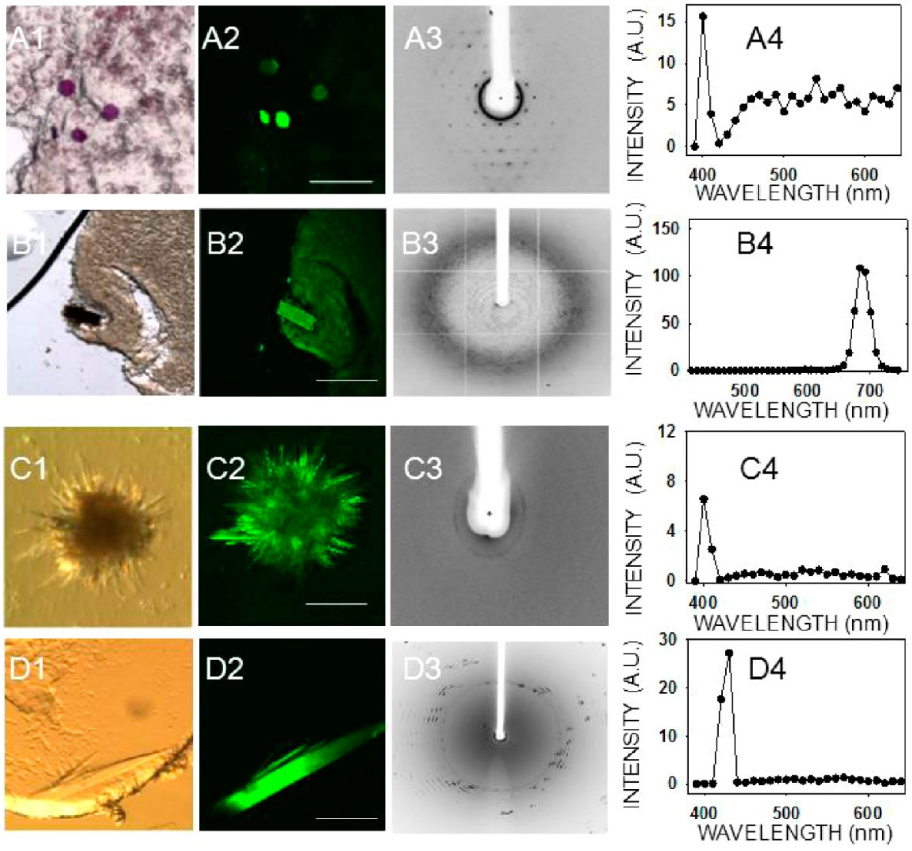

Figure 2. TPM imaging of membrane protein crystals in a mesophase. Bright field images (1), TPM images (2), X-ray diffraction images (3), and two-photon-excited emission spectra (4) of membrane protein crystals in a mesophase: (A) bacteriorhodopsin, (B) RC crystals, and (C and D) 5-HT4R crystals grown from mesophase trials. Spectra in panels A4 and C4 were recorded with 810 nm excitation and those in panels B4 and D4 at 850 nm excitation. Scale bars are 150 μm (A2, C2, and D2) and 300 μm (B2).

noted. Maximizing peak laser pulse power while keeping the average laser power constant by incorporating dispersion compensation improved signal intensities by 36% relative to the case with only minimal compensation (Figure 1B). Considering that fluorescence generated by a linear, single-photon process does not inversely depend on the duration of the pulse for the same average laser power,[29] we indirectly confirmed that the images observed were generated by a nonlinear, two-photon process. To identify whether the image images with little or no background noise resulting from their SHGwas generated by SHG or TPEF for each crystal, we also obtained the emission spectrum. A sharp SHG peak should occur at exactly half the excitation wavelength, whereas fluorescence emission was expected over a wider range of wavelengths.

Imaging Mesophase Crystallization Setups. Mesophase crystallization trials were performed with three membrane proteins. Bacteriorhodopsin crystals in a mesophase could easily be viewed by bright field microscopic imaging because of their deep purple color (Figure 2, A1). Bacteriorhodopsin crystals (10 μm × 10 μm × 10 μm) in a mesophase also were readily detected by TPM because they yielded high-contrast images with little or no background noise because of their SHG activity (Figure 2, A2). The same crystals provided a weak TPEF signal as well (Figure 2, A4).

Because of their dark brown color, RC crystals were readily visualized in a mesophase under a bright field microscope (Figure 2, B1) and by TPM imaging (Figure 2, B2). A clear TPEF emission spectrum was recorded from these crystals, although there was no SHG (Figure 2, B4). The visible fluorescence emission from RC crystals had an atypical profile compared to those of all other protein crystals imaged in this work, as described below. Emission at 480−530 nm was largely absent, although strong emission at ∼683 nm was detected. This shift is most probably due to the two-photon absorption of the 850 nm incident light by the intrinsic RC chromophores, which have a complex absorption and emission spectra.[30] It is possible that the absence of a SHG peak is also related to the presence of these chromophores, because any 425 nm light generated by a SHG process could be reabsorbed by such chromophores. We also examined crystals grown during mesophase crystallization trials with 5-HT4R. In one case, we found low-resolution diffraction (∼30−40 Å) for a bundle of needles (Figure 2, C1 and C3) and, in another case, a thin plate with a *d* spacing of ∼5 Å (Figure 2, D1 and D3). Both crystal types showed a distinct SHG and a weak TPEF signal (Figure 2, C4 and D4), but we were unable to determine the space group or confirm the identity of these crystals because of the poor resolution of diffraction.

SHG in Nonprotein Crystals. Though SHG was useful for detecting protein crystals, other chiral or achiral molecules can give rise to false positives in protein crystallization trials. Figure S1 (Supporting Information) depicts an example of a small organic molecule (Figure S1A), and inorganic crystals (Figure S1B), with second-harmonic activity.

dx.doi.org/10.1021/bi201682q | *Biochemistry* 2012, 51, 1625−1637

Despite it being a non-chiral molecule, crystals of GR125487, a 5-HT4R antagonist, displayed strong SHG (Figure S1A of the Supporting Information, 1−4). To confirm the presence of SHG, we illuminated this crystal with light at three different wavelengths, and in each case, a spike was registered at half the wavelength of the incident light. In addition, TPEF with maxima at ∼480 and ∼530 nm was observed. Energies of the excitation beam at the three different wavelengths were not equalized in this experiment.

Figure S1B of the Supporting Information shows crystals of KH_2PO_4, an inorganic buffer commonly used in protein crystallization trials. KH_2PO_4 crystals, known for their SHG activity, predictably produced SHG but no TPEF (Figure S1 of the Supporting Information, B4). We tested several other salt crystals as negative controls [NaCl, $CuSO_4$, $NiSO_4$, and $(NH_4)_2SO_4$], and, as expected, none of them produced SHG or TPEF signals (data not shown).

TPM Imaging of Protein Crystals in Major Lattice Systems. We grew 13 crystal forms of 11 different proteins and confirmed their identities and space groups by indexing and data processing (10 of the crystal forms are listed in Table 1, whereas three of them are not shown). These crystals then were tested for their second-order NLO activity. The results are shown in Figure 3 and Table 1. Lysozyme crystals grown in a triclinic crystal system (Figure 3, row A) and endo-1,4-β-D-xylanase II in a monoclinic system (Figure 3, row B) were the only two protein crystals that exhibited strong SHG. Neither of the tetragonal protein crystals, i.e., lysozyme or thaumatin (Figure 3, rows C and D, respectively), produced SHG, but both displayed a clear TPEF, similar to that observed for GR125487. Protein crystals belonging to a trigonal lattice (data not shown), cubic lattice (data not shown), hexagonal space group [RPE65 (Figure 3E)], or orthorhombic lattice [glucose isomerase (Figure 3F)] also had similar TPEF emission but no SHG. Crystals of RPE65 and RNase A, belonging to an orthorhombic system, were especially unresponsive to TPM imaging (Figure 3G,H). We observed an inverse correlation of SHG with crystallographic symmetry. In addition, most protein crystals exhibited fluorescence with peaks at ∼480 and ∼530 nm that allowed them to be imaged by TPEF. Finally, we imaged trigonal crystals of ground-state and photoactivated rhodopsin (Figure 4A). Bovine rhodopsin is another atypical case because it has a covalently attached chromophore (11-*cis*-retinal) contributing to the emission spectrum in the visible range. The absorption maximum for ground-state rhodopsin in solution is ∼500 nm, whereas its fluorescence emission is strongly dependent on the excitation wavelength.[31] When rhodopsin crystals were excited at 910 nm, the TPEF maximum of ground-state rhodopsin was ∼585 nm, but after photoactivation causing isomerization of 11-*cis*-retinal to all-*trans*-retinal, a blue shift and a decrease in the intensity of fluorescence emission occurred (Figure 4B). The maximum in the difference emission spectrum of rhodopsin (ground state minus photoactivated state) was ∼600 nm (Figure 4C), in good agreement with the reported value for the single-photon fluorescence of solubilized rhodopsin in the ground state.[31] At 910 nm excitation, most of the fluorescence emission of ground-state rhodopsin should stem from the bound 11-*cis*-retinal. In contrast, when the crystals were excited with a wavelength of 730 nm, the contribution of 11-*cis*-retinal to the emission spectrum was significantly reduced, and it then resembled those of other protein crystals analyzed in this work with peaks at ∼480 and ∼530 nm (Figure 4D). Nonetheless, the difference emission spectrum with excitation at 730 nm (Figure 4E) shows a maximum at ∼600 nm and a minimum at ∼475 nm, most probably derived from 11-*cis*-retinal and all-*trans*-retinal, respectively.

In addition to data obtained in the epi configuration, we also used transmission geometry to obtain TPM images of tetragonal lysozyme crystals to compare the sensitivity of the microscope in these two possible configurations. Transmission and epi images shown in Figure S2 (Supporting Information) were obtained simultaneously. Considering that both epi and transmission detection paths employ the same type of detector, and that to obtain a brighter image in the transmission mode, the gain on the detector was double that used for epi detection, we failed to improve contrast by using the transmission configuration.

Two-Photon Excitation Spectrum of Tetragonal Lysozyme Crystals. To optimize the imaging of protein crystals exhibiting no SHG and learn more about this phenomenon, we measured the excitation spectrum of a tetragonal lysozyme crystal. This crystal system was chosen because no SHG was seen at any wavelength; thus, the total fluorescence could be compared at different excitation wavelengths. Results shown in Figure 5B suggest that there is one TPM excitation peak close to 730 nm and a second peak near 810 nm. With our experimental setup, it was not possible to obtain an emission spectrum at shorter wavelengths because of the limited tunable range of our laser. Figure 5C displays the

Table 1. Protein Crystal Systems and Their NLO Properties[a]

No.	Protein and crystal system	Space group	Protein Data Bank (PDB) entry	SHG	Fluorescence
1	lysozyme (triclinic)	$P1$	7LYZ	+	+
2	endo-1,4-β-D-xylanase II (monoclinic)	$C2$	1XYN	+	+
3	lysozyme (tetragonal)	$P4_32_12$	2LZM	−	+
4	thaumatin (tetragonal)	$P4_12_12$	2PE7	−	+
5	RPE65 (hexagonal)	$P6_5$	3KVC	−	+
6	glucose isomerase (orthorhombic)	$I222$	6XIA	?	+
7	ribonuclease A (orthorhombic)	$P2_12_12_1$	1RTA	−	−
8	bacteriorhodopsin (hexagonal)[b]	$P6_3$	1AP9	+	+
9	photosynthetic reaction center (tetragonal)	$P4_32_12$	6PRC	−	+
10	rhodopsin (trigonal)	$P3_112$	2I37	?	+

[a]Protein crystals were identified by their X-ray diffraction patterns, and their assignment to space groups was accomplished by crystallographic data processing. These crystals were further assessed for their SHG properties by using TPM imaging as described in Experimental Procedures. Unless otherwise stated, the excitation wavelength for these experiments was 850 nm. A plus or minus sign indicates a SHG or a TPEF signal observed (+) or not (−), respectively. A question mark indicates that SHG was too weak to be confirmed unambiguously. The third column shows the PDB entries of protein crystal structures deposited by our laboratory or others that correspond to the protein crystal systems used in this study. [b]Space group determination was not performed in this study.

dx.doi.org/10.1021/bi201682q | *Biochemistry* 2012, 51, 1625−1637

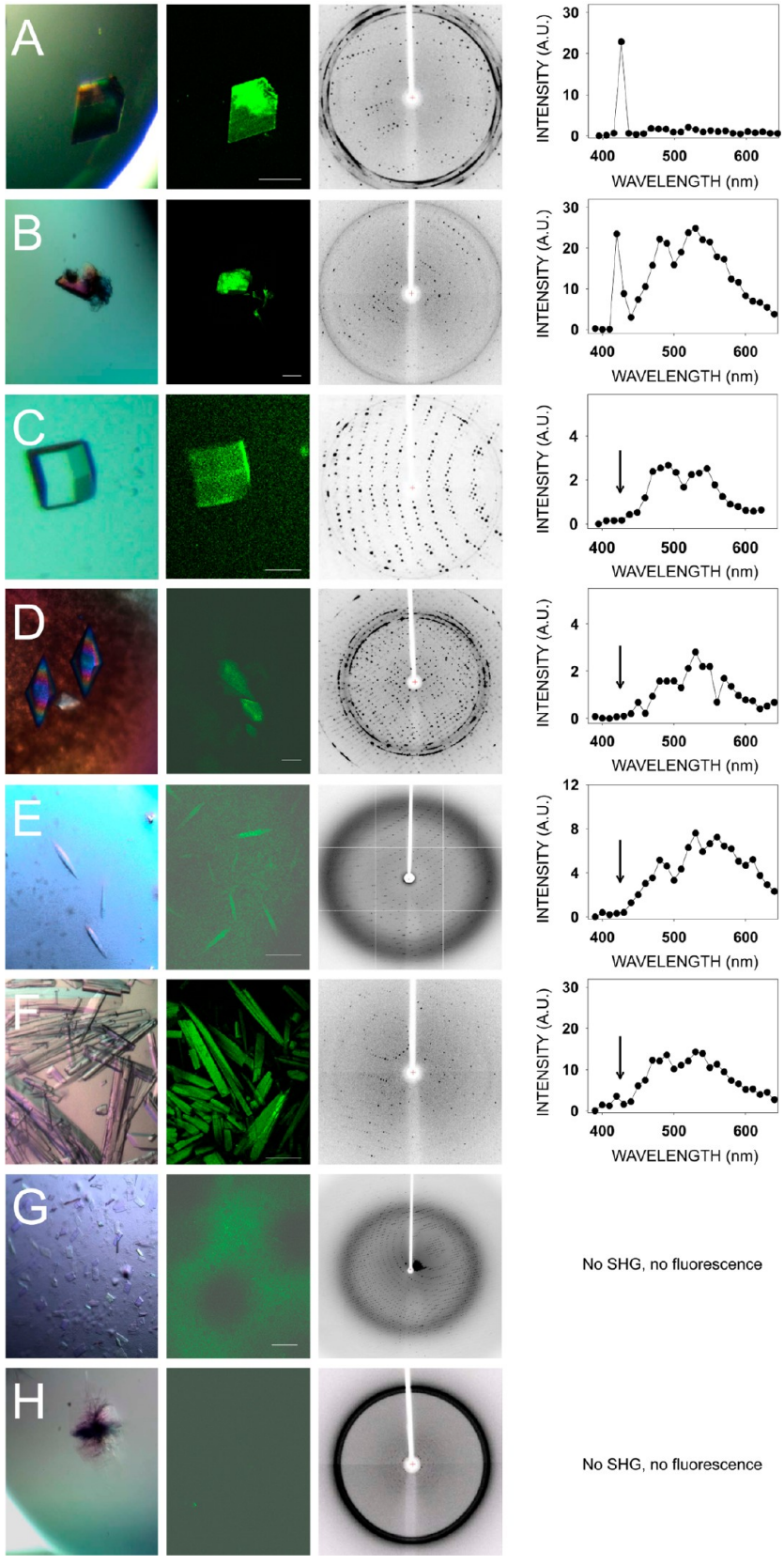

Figure 3. TPM imaging of protein crystals in major crystal systems. Shown from left to right are bright field images, TPM images, diffraction images, and corresponding emission spectra, respectively, from eight different protein crystals representing major protein crystal systems: (A) lysozyme (triclinic), (B) endo-1,4-β-D-xylanase II from *Trichoderma* sp. (monoclinic), (C) lysozyme (tetragonal), (D) thaumatin from *Thaumatococcus daniellii* (tetragonal), (E) bovine RPE 65 kDa protein (hexagonal), (F) glucose isomerase from *S. rubiginosus* (orthorhombic), (G) bovine RPE65 (orthorhombic), and (H) ribonuclease A from bovine pancreas (orthorhombic). Scale bars in TPM images are 150 μm.

dx.doi.org/10.1021/bi201682q | *Biochemistry* 2012, 51, 1625−1637

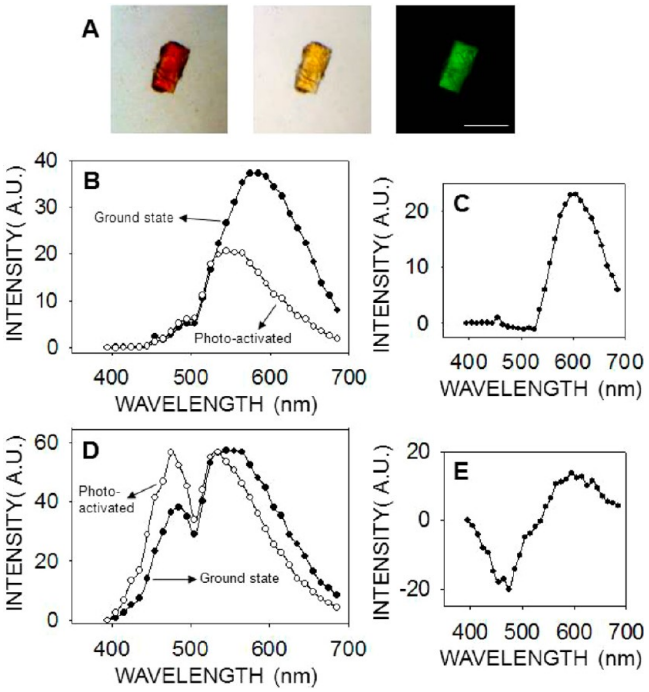

Figure 4. TPM imaging of rhodopsin crystals. (A) Trigonal rhodopsin crystals were imaged with a bright field microscope before (left) and after photoactivation (center). In the TPM image (730 nm excitation wavelength), smaller rhodopsin crystals are visible over a larger crystal (right). The scale bar is 150 μm. (B and D) Emission spectra of rhodopsin crystals in the ground state (●) and after photoactivation (○), with an excitation wavelength of 910 (B) or 730 nm (D). (C and E) Difference emission spectra of rhodopsin crystals (ground state minus photoactivated state) with an excitation wavelength of 910 (C) or 730 nm (E).

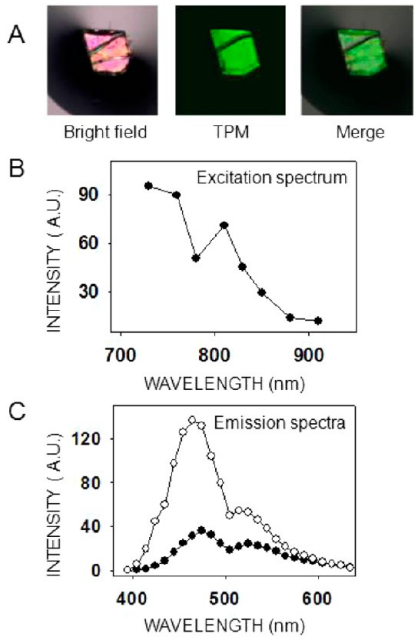

Figure 5. Excitation and emission spectra of a tetragonal lysozyme crystal. (A) The lysozyme crystal was imaged with either a bright field microscope (left) or a two-photon microscope with an excitation wavelength of 730 nm (center). The two images are merged at the right. (B) Two-photon excitation spectrum of a tetragonal lysozyme crystal. Because no SHG was observed, the total emitted light was plotted for each excitation wavelength. Laser power settings were adjusted to deliver the same energy at every excitation wavelength. (C) Emission spectra of a lysozyme tetragonal crystal at two different excitation wavelengths, 760 (○) and 850 nm (●).

emission spectra at two different excitation wavelengths, 760 and 850 nm. Similar to that of GR125487 crystals, the relative intensity of the peaks at ~480 and ~530 nm varied with excitation wavelength. This and the presence of at least two peaks in the excitation spectrum of lysozyme suggest the presence of at least two fluorophores, or two excitation states of one fluorophore. Finally, tetragonal lysozyme crystals were broken into smaller pieces to disperse them in the drop of mother liquor so we could image different pieces at different angles relative to the laser beam. Still, we did not observe SHG or significant changes in TPEF intensity (not shown). This result fails to confirm the angle dependence known to affect SHG intensity from crystals.[8]

TPM Imaging of Aromatic Amino Acid Crystals. The wavelength range of fluorescence emission we observed from protein crystals (400−600 nm) did not seem to emanate from the well-characterized intrinsic fluorescence of aromatic amino acid residues. However, the excitation peaks of lysozyme (~730 and ~810 nm) could correspond to three-photon excitation of such aromatic residues (absorption maxima in water of 257 nm for Phe, 274 nm for Tyr, and 280 nm for Trp). To rule out this possibility, we imaged crystals of these amino acids in monomeric form (Figure S3 of the Supporting Information). Strong SHG activity, as expected,[32] but little or no fluorescence in the visible light range was noted in each case. This observation suggests that the observed fluorescence from protein crystals was not derived from their aromatic amino acids through a three-photon process. This result is also notable because aromatic amino acids are sometimes used as additives for protein crystallization and, therefore, could be responsible for SHG false positives in protein crystallization trials.

Increased TPEF from Lysozyme Crystals Treated with APS. Intrigued by the anecdotal observation that older crystals generally show more intense TPEF than fresh crystals (e.g., see Figure 6A,C,D), we hypothesized that oxidation of the proteins could be partly responsible for this increase. Incubation of fresh tetragonal lysozyme crystals with APS (a known oxidizing agent acting via free radicals) for 2 days produced a dramatic increase in TPEF (Figure 6B) of the same order of magnitude as that noted in 1−2-year-old crystals (Figure 6E). Incubation of a crystal with 17 mM APS induced a significant increase in fluorescence intensity in just 20 min, without modifying the shape of the TPEF spectrum (Figure S4 of the Supporting Information).

Next we performed a series of experiments to determine if this APS-induced increase in visible fluorescence is a NLO process limited to crystal lattices or could be reproduced in solution and/or by a linear optical process.

Because the maximal two-photon excitation of lysozyme crystals was seen in the 730−810 nm range (lower excitation wavelengths were not available on our two-photon microscope), we first investigated whether APS could induce an increase in the UV absorbance of proteins in solution. Incubation of lysozyme for 6 h with 1−2 mM APS in solution was sufficient to observe a clear increase in absorbance in the 300−400 nm range, in a pH-dependent manner (Figure S5 of the Supporting Information).

dx.doi.org/10.1021/bi201682q | *Biochemistry* 2012, 51, 1625−1637

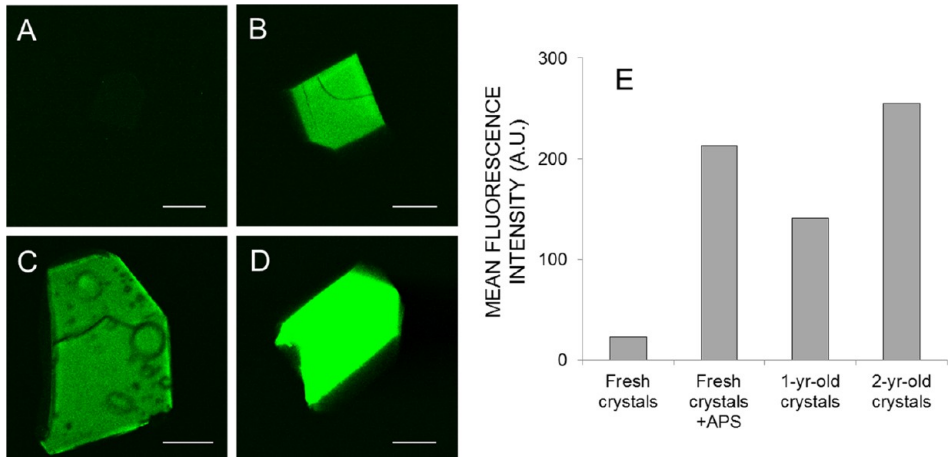

Figure 6. TPM fluorescence of fresh and aged tetragonal lysozyme crystals: TPM images of a fresh (3-day-old) crystal (A), a fresh APS-treated crystal (B), a 1-year-old crystal (C), and a 2-year-old crystal (D). The laser power at 810 nm and detector settings were identical for all four images. The mean fluorescence intensity from each crystal is shown in panel E. For panel B, 25 mM APS was added to the 1-day-old lysozyme crystal, which was then incubated for an additional 2 days before imaging. As in previous experiments, no SHG was observed for these tetragonal lysozyme crystals (not shown). Scale bars in the four images are 150 μm.

In a similar experiment, we also found a dramatic increase in one-photon excitation of lysozyme in the UV-A range upon APS treatment (Figure S6A of the Supporting Information), with the resulting increase in visible fluorescence emission having a maximum at ~450 nm (Figure S6B of the Supporting Information). Careful analysis of the spectra revealed that the non-APS-treated lysozyme sample also evidenced a weak fluorescent emission with an ~450 nm maximum, in good agreement with that of concentrated protein solutions.[33] The last value could reflect a small percentage of oxidation in fresh lysozyme samples.

Next we explored the possibility that the observed visible, one-photon and two-photon fluorescence emission could originate from oxidized aromatic amino acids (Ar aas). Amino acids generate multiple derivatives upon oxidation by free radicals,[34] and Trp especially is known to produce products that fluoresce in the visible range.[35] Initially, we imaged a drop containing a mixture of Trp, Phe, and Tyr via TPM. As with lysozyme crystals, a rapid increase in TPEF was observed upon addition of APS (Figure S7B of the Supporting Information, right-bottom drop), while its emission spectrum resembled that of most protein crystals (Figure S7C of the Supporting Information) (maxima at ~485 and ~545 nm). Finally, to elucidate the individual contribution of each aromatic amino acid, we measured the UV-A absorbance and one-photon fluorescence of the Ar aas upon treatment with APS. As with lysozyme, a large increase in absorbance and visible fluorescence emission were noted, but only when Trp was present (Figure S8 of the Supporting Information). The one-photon fluorescence maximum of Trp was similar to that of lysozyme, and it was present even in non-APS-treated samples, although to a much lesser extent (Figure S8B of the Supporting Information, inset), in agreement with the weak TPEF noted for fresh Trp crystals (Figure S3A of the Supporting Information). The increase in the fluorescence of Phe and Tyr upon treatment with APS was barely measurable under our experimental conditions (Figure S8B of the Supporting Information, inset).

A Second-Order Process Generates Visible Fluorescence in Protein Crystals. To confirm that the source of the observed fluorescence was a two-photon rather than a three-photon excitation process, we measured the dependence of the fluorescence signal on laser power in crystals of glucose isomerase, xylanase (Figure 7A), and tetragonal lysozyme (Figure 7B) crystals. Then, we determined the order of the process from slopes of lines fitted to data on logarithmic plots of fluorescence as a function of laser power. In each case, the slope was within the range of 1.88−2.15, consistent with a two-photon process. The signal from xylanase crystals, which is composed of both second harmonic and fluorescence (Figure 3B), was also proportional to the second power and consistent with a two-photon process.

TPEF from Protein Crystals Increases after Their Exposure to Different Fluorophores. We found that after exposure to fluorescent dyes, two-photon-excited fluorescence from tetragonal lysozyme crystals also increased significantly (Figure 8A) in a time-dependent manner. A lysozyme crystal exposed to DAPI (Figure 8B) had a maximal fluorescence at 475 nm, and its spectrum resembled that of a lysozyme crystal before exposure to a fluorescent dye [Figure 8C (□)] with a maximum at 465 nm and that of DAPI itself, which exhibits one-photon maximal fluorescence at 461 nm (not shown). Even though the fluorescence from a lysozyme crystal increased more than 6 times over the 15 min incubation time with fluorescein (Figure 8A), this dye did not penetrate well inside the crystal. Instead, the spectrum measured at the edge of the crystal closely resembled the spectrum from fluorescein, whereas the spectrum taken from inside of the crystal was almost identical to that measured before its exposure to a fluorescent dye (Figure 8C). Finally, the spectrum from inside the lysozyme crystal exposed to NBD PC resembled that from the NBD PC solution (Figure 8D), indicating that after exposure for 15 min, this dye penetrated inside the lysozyme crystal.

■ DISCUSSION

SHG and its application to biological imaging have been extensively studied.[36−38] Pioneering work in imaging protein crystals with TPM has demonstrated the ability of SONICC to detect protein crystals in a highly nonuniform suspension of a lipidic cubic phase. Kissick et al. systematically documented the superiority of SONICC for detecting microcrystals by using

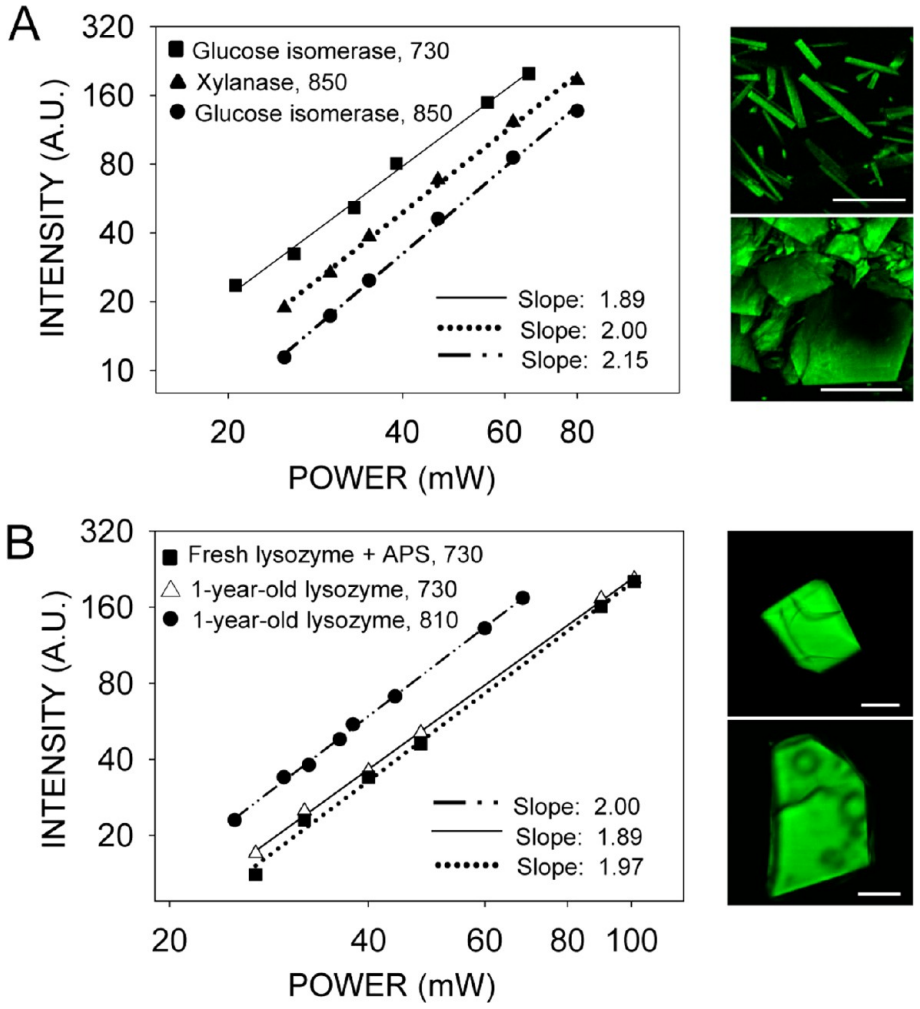

Figure 7. Logarithmic plots of fluorescence intensity as a function of excitation power indicate a two-photon excitation process. (A) Vapor diffusion-grown crystals of glucose isomerase and xylanase. Excitation wavelengths in nanometers are indicated next to the protein name in the top left corner of the graph. Examples of TPM images are shown next to the graph: (top) glucose isomerase excited at 730 nm and (bottom) xylanase excited at 850 nm. (B) One-year-old and fresh APS-aged tetragonal lysozyme crystals. Excitation wavelengths in nanometers are indicated next to the protein name in the top left corner of the graph. Examples of TPM images are shown next to the graph: (top) fresh lysozyme crystal incubated with 25 mM APS for 2 days before TPM imaging at 730 nm and (bottom) 1-year-old lysozyme crystal imaged at 810 nm. The fitted slopes are represented in the bottom right corners of each graph; in each case, r^2 was >0.995. Scale bars in the four images are 150 μm.

automated imaging and particle counting in mesophase crystallization trials.[4] Our aim was to employ these established techniques to assess various protein crystallization trials being conducted in our laboratory. In our analysis, crystal identification in mesophase trials with nonlinear imaging proved to be capable of identifying crystals as small as 10 μm × 10 μm × 10 μm, but other than identifying crystals, one of the most critical questions addressed was whether the observed SHG from these microcrystals stemmed from their proteinaceous nature as suggested by previous studies.[8] Identification of protein crystals at the screening stage of crystallization trials is critical for successful results, which otherwise would translate into missing perfectly good leads or wasted effort optimizing false positives.

Small chiral molecules are known to form noncentrosymetric crystals with NLO properties,[39] which can constitute false positives in protein crystal trials. We show examples of small molecules with strong SHG activity: Trp, Phe, Tyr, KH_2PO_4, and GR125487 (the last is a small achiral pharmacological agent). Even though SHG imaging is a powerful method for imaging small protein crystals in turbid media, its limitations in identifying protein crystals must be considered. Another problem with SHG-only imaging of protein crystals is the abundance of false negatives. Thus, of 13 crystal forms representing the seven major chiral classes, only three exhibited strong SHG activity.

Previous studies theoretically analyzed the NLO proprieties of various protein crystals by using NLOPredict plugin [incorporated into molecular graphics software UCSF Chimera (http://plato.cgl.ucsf.edu/chimera/)].[39,40] Moreover, the properties of SHG in chiral systems also were extensively studied and defined (reviewed in refs 4 and 10). According to these theoretical assumptions, NLO properties will vary depending on how individual molecules are arranged with respect to various symmetry operators in different crystal classes, with lower symmetry generally corresponding to higher SHG, which is theoretically forbidden for centrosymmetric and highly symmetric cubic 432 crystals.[41]

To address critical aspects of crystal symmetry and SHG from protein crystals, knowledge of the classical definitions for some of the major crystal lattice systems and other terms of interest is required. All crystal systems can be broadly separated

dx.doi.org/10.1021/bi201682q | *Biochemistry* 2012, 51, 1625−1637

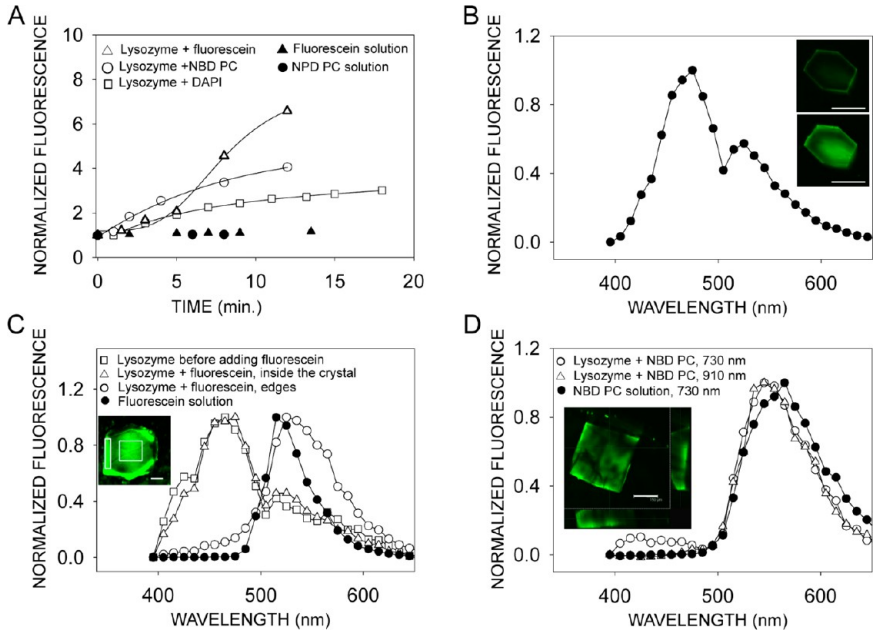

Figure 8. Characterization of tetragonal lysozyme crystals exposed to different fluorescent dyes. (A) The fluorescence of lysozyme crystals increases with time after their exposure to solutions of fluorescent dyes, NBD PC, fluorescein, and DAPI. Fluorescence from drops of the solutions did not change over the same period of time. The total fluorescence from crystals was normalized to that measured immediately before addition of dye solutions to the crystals. Fluorescence from solution drops was normalized to the time immediately after placing the solution drop on the coverslip-bottom dish in front of the microscope objective. (B) Fluorescence of a lysozyme crystal exposed for 20 min to 60 μM DAPI. The inset shows TPM images of a lysozyme crystal immediately after exposure to DAPI (top) and 9 min after exposure (bottom). (C) Spectral characteristics of a lysozyme crystal exposed to 50 μM fluorescein. The normalized spectrum from the crystal obtained before adding fluorescein overlaps with the spectrum from an area inside the crystal (indicated by a square in the inset) obtained after exposure to fluorescein for 15 min. The spectrum from fluorescein in solution closely resembles the spectrum taken from the edge of the crystal (indicated by a rectangle in the inset) after exposure to fluorescein. (D) Fluorescence of a lysozyme crystal exposed for 15 min to 133 μM fluorescently labeled phospholipid NBD PC. The normalized spectrum from the crystal exposed to solution, obtained at 730 nm, indicated with empty circles, overlaps with the spectrum obtained at 910 nm, indicated with empty triangles. The spectrum obtained with 730 nm from NBD PC in solution, indicated with filled circles, is red-shifted 20 nm. The inset shows data obtained from a series of z-slice images of a lysozyme crystal exposed to NBD PC obtained along the axis perpendicular to the crystal face. The main panel shows image halfway through the crystal thickness. The two cross sections, shown at the bottom and at the right, indicate that the highest fluorescence is at the edges of the crystal. Scale bars in all images are 150 μm.

into centrosymmetric or noncentrosymmetric classes. A centrosymmetric crystal system has an inversion center as one of its symmetry elements, and in such a system, every point (say x, y, z) in the unit cell has a corresponding indistinguishable point ($-x$, $-y$, $-z$). Crystals with such inversion center symmetry do not evidence certain physical properties such as the piezoelectric effect.[41,42] Proteins crystallize in noncentrosymmetric space groups, and the capability of noncentrosymmetric crystal systems to display NLO properties (with the exception of cubic 432 crystals) allows their detection in highly nonhomogeneous backgrounds by TPM techniques.

However, additional factors can weaken an NLO response. (i) SHG depends on the angle of incidence of the laser beam relative to the crystallographic axis. (ii) Crystals of disparate sizes and density behave differently depending on the geometry of the microscope used to collect SHG, i.e., a transmission or epi configuration.[8] These limitations pose serious obstacles to the general applicability of this technique for protein crystal imaging and screening. Moreover, we noted that almost all the protein crystals tested exhibited fluorescence in the visible range, and this was actually what allowed the imaging of SHG-silent crystals. However, the fluorescence signal-to-noise ratio obtained for different crystals was variable and often not reproducible for the same crystals imaged at different times. Intrinsic blue-green fluorescence emission upon excitation with UV-A light was previously observed for proteins in solution,[33] protein crystals and aggregates,[43] protein fibrils and matrix proteins,[44,45] and triethylamine and dendrimers containing amine/amide or imine groups (ref 46 and references cited therein). However, to the best of our knowledge, blue-green TPEF has not been used before to image protein crystals.

Two different hypotheses have been proposed to explain the rarely reported blue-green fluorescent emission of proteins and other amine/amide-containing polymers: (i) delocalization of peptide electrons by intra− and intermolecular hydrogen bond formation[43,44] and (ii) transfer of charge between amine groups and molecular oxygen.[46,47] In the latter case, the hypothesis is supported by the observation that blue-green fluorescence emission increased upon the treatment of polymers with oxygen or other oxidizing agents.

We set up a series of experiments to elucidate the origin of this blue-green TPEF. These experiments provide evidence that this phenomenon is not an artifact of our TPM system and can be produced by different mechanisms.

(1) Laser power versus intensity plots demonstrated that the luminescence emanating from three different protein crystals is generated by a second-order optical process.

(2) A multiple-factor approach using absorbance, one-photon fluorescence, and TPEF of lysozyme and aromatic amino acids in solution suggests that Trp oxidation via free radicals is, at least in part, responsible for the TPEF observed in

dx.doi.org/10.1021/bi201682q | *Biochemistry* 2012, 51, 1625−1637

most protein crystals. This could explain several observations: (i) the high variability in the intensity but high reproducibility of the shape of TPEF spectra from unrelated protein crystals, (ii) the slow (i.e., year-long) increase in fluorescence for different protein crystals, which is expected to be dependent on temperature, pH, light exposure, crystallization plasticware, protein identity, etc., (iii) the lack of TPEF from RNase A, a protein lacking Trp, and (iv) the TPEF of GR125487 that may originate from a mechanism similar to that involving Trp, because this molecule contains a fluoro-indole group. The fact that the two-photon excitation and emission spectra of APS-oxidized lysozyme and Trp do not coincide exactly with their corresponding one-photon spectra is not surprising, as this is common for many proteins and dyes in solution.[48,49]

(3) Finally, Raman spectroscopy of protein crystals requires fresh crystals (<3 months old) to maintain a high signal-to-noise ratio, because the autofluorescence from old crystals generates a high background upon excitation with a red laser (647 nm).

Additionally, we found that addition of fluorescent dyes with no particular affinity for lysozyme can stain lysozyme crystals in a few minutes. This result suggests that in some instances fluorescent contaminants could account for the TPEF of protein crystals. For example, color dyes commonly used in pH standards can interfere with fluorescence experiments with proteins in buffered solutions (unpublished). On the other hand, this finding provides the opportunity to use different fluorescent dyes at trace concentrations to enhance the detection of protein crystals by TPM, or the use of TPM to follow the soaking of protein crystals with ligands.

Results of this study emphasize the need to thoroughly evaluate each of the various methods employed for crystal detection in protein crystallization trials. Such techniques include (1) light microscopy and birefringence, (2) UV absorption and fluorescence detection, and (3) SONICC. Each has its merits and shortcomings. The first method, involving bright field microscopy and crossed polarizers, still works well in most cases where crystal sizes are not too small, but it is prone to false positives. UV detection of aromatic protein residues offers a direct method for identifying protein crystals but lacks sensitivity, exhibits poor transmission through plastics, and can damage precious samples.[5] Recently, two-photon-excited UV fluorescence was reported to have improved transmission through plastics and turbid media,[9] but this still retains poor sensitivity with the potential of damaging crystals. In our experimental setup, the combination of SHG and intrinsic visible TPEF provided a noninvasive, highly sensitive detection of microcrystals with sizes as small as 10 μm × 10 μm × 10 μm against highly birefringent backgrounds. Using this technique, we found that imaging most protein crystals was possible because of their TPEF in the blue−green range rather than their SHG.

Proteins with cofactors (rhodopsin and RC) have altered emission spectra compared with those of proteins without cofactors. In the case of bacteriorhodopsin, the fluorescence excitation and emission maxima fall outside the range used in this work, and therefore, the contribution of its retinal to the spectrum was minor or negligible.

In summary, the limitations of SHG imaging of protein crystals stem from proven SHG positive signals derived from small molecule crystals and a lack of SHG from many protein crystals. Nevertheless, detection of small crystals in turbid media through an UV-absorbing plastic barrier with non-damaging infrared light by a single instrument makes the combination of SHG and intrisic TPEF useful for early protein crystal identification and imaging during crystallization trials. This dual-detection mode could employ a single excitation wavelength (~810 nm) or excitation wavelengths for TPEF and SHG detection optimized for the particular protein crystals being analyzed.

■ ASSOCIATED CONTENT

Supporting Information

TPM images, TPEF spectra, and bright field images of small molecule and protein crystals and one- and two-photon emission fluorescence and absorbance spectra of aromatic amino acids and lysozyme in solution. This material is available free of charge via the Internet at http://pubs.acs.org.

■ AUTHOR INFORMATION

Corresponding Author

*Phone: (216) 368-4631. Fax: (216) 368-1300. E-mail: kxp65@case.edu.

Author Contributions

P.P. and G.P. contributed equally to this work.

Funding

This research was supported, in whole or in part, by National Institutes of Health Grants EY009339 and P30 EY11373. K.P. is the John H. Hord Professor of Pharmacology.

Notes

The authors declare no competing financial interest.

■ ACKNOWLEDGMENTS

We thank Dr. Leslie T. Webster, Jr., Philip D. Kiser, David T. Lodowski, and Marcin Golczak for critical comments about the manuscript. We also thank P. D. Kiser, D. T. Lodowski, and M. Golczak for providing protein crystals for this work.

■ ABBREVIATIONS

5−HT4R, serotonin type 4 receptor; APS, ammonium persulfate; Ar aas, amino acids; DAPI, 4′,6-diamidino-2-phenylindole dilactate; GR125487, 5-fluoro-2-methoxy(1-{2-[(methylsulfonyl)amino]ethyl}-4-piperidinyl)-1*H*-indole-3-methylcarboxylate sulfamate; HEPES, 4-(2-hydroxyethyl)-piperazine-1-ethanesulfonic acid; GVD, group velocity dispersion; NA, numerical aperture; NLO, nonlinear optical; NBD PC, 1-hexanoyl-2-{6-[(7-nitro-2-1,3-benzoxadiazol-4-yl)-amino]hexanoyl}-*sn*-glycero-3-phosphocholine; PMT, photomultiplier tube; RC, photosynthetic reaction center; RNase A, ribonuclease A; RPE, retinal pigmented epithelium; RPE65, RPE-specific 65 kDa protein; SHG, second-harmonic generation; SONICC, second-order NLO imaging of chiral crystals; TPEF, two-photon-excited fluorescence; TPM, two-photon microscopy.

■ REFERENCES

(1) Cherezov, V., Rosenbaum, D. M., Hanson, M. A., Rasmussen, S. G., Thian, F. S., Kobilka, T. S., Choi, H. J., Kuhn, P., Weis, W. I., Kobilka, B. K., and Stevens, R. C. (2007) High-resolution crystal structure of an engineered human β2-adrenergic G protein-coupled receptor. *Science 318*, 1258−1265.

(2) Wu, B., Chien, E. Y., Mol, C. D., Fenalti, G., Liu, W., Katritch, V., Abagyan, R., Brooun, A., Wells, P., Bi, F. C., Hamel, D. J., Kuhn, P., Handel, T. M., Cherezov, V., and Stevens, R. C. (2010) Structures of

the CXCR4 chemokine GPCR with small-molecule and cyclic peptide antagonists. *Science 330*, 1066−1071.
(3) Cherezov, V., Hanson, M. A., Griffith, M. T., Hilgart, M. C., Sanishvili, R., Nagarajan, V., Stepanov, S., Fischetti, R. F., Kuhn, P., and Stevens, R. C. (2009) Rastering strategy for screening and centring of microcrystal samples of human membrane proteins with a sub-10 micron size X-ray synchrotron beam. *J. R. Soc., Interface 6* (Suppl. 5), S587−S597.
(4) Kissick, D. J., Gualtieri, E. J., Simpson, G. J., and Cherezov, V. (2010) Nonlinear optical imaging of integral membrane protein crystals in lipidic mesophases. *Anal. Chem. 82*, 491−497.
(5) Gill, H. S. (2010) Evaluating the efficacy of tryptophan fluorescence and absorbance as a selection tool for identifying protein crystals. *Acta Crystallogr. F66*, 364−372.
(6) Judge, R. A., Swift, K., and Gonzalez, C. (2005) An ultraviolet fluorescence-based method for identifying and distinguishing protein crystals. *Acta Crystallogr. D61*, 60−66.
(7) Dierks, K., Meyer, A., Oberthur, D., Rapp, G., Einspahr, H., and Betzel, C. (2010) Efficient UV detection of protein crystals enabled by fluorescence excitation at wavelengths longer than 300 nm. *Acta Crystallogr. F66*, 478−484.
(8) Wampler, R. D., Kissick, D. J., Dehen, C. J., Gualtieri, E. J., Grey, J. L., Wang, H. F., Thompson, D. H., Cheng, J. X., and Simpson, G. J. (2008) Selective detection of protein crystals by second harmonic microscopy. *J. Am. Chem. Soc. 130*, 14076−14077.
(9) Madden, J. T., Dewalt, E. L., and Simpson, G. J. (2011) Two-photon excited UV fluorescence for protein crystal detection. *Acta Crystallogr. D67*, 839−846.
(10) Haupert, L. M., and Simpson, G. J. (2009) Chirality in nonlinear optics. *Annu. Rev. Phys. Chem. 60*, 345−365.
(11) Imanishi, Y., Batten, M. L., Piston, D. W., Baehr, W., and Palczewski, K. (2004) Noninvasive two-photon imaging reveals retinyl ester storage structures in the eye. *J. Cell Biol. 164*, 373−383.
(12) Palczewska, G., Maeda, T., Imanishi, Y., Sun, W., Chen, Y., Williams, D. R., Piston, D. W., Maeda, A., and Palczewski, K. (2010) Noninvasive multiphoton fluorescence microscopy resolves retinol and retinal condensation products in mouse eyes. *Nat. Med. 16*, 1444−1449.
(13) Mohler, W., Millard, A. C., and Campagnola, P. J. (2003) Second harmonic generation imaging of endogenous structural proteins. *Methods 29*, 97−109.
(14) Oesterhelt, D., and Stoeckenius, W. (1974) Isolation of the cell membrane of *Halobacterium halobium* and its fractionation into red and purple membrane. *Methods Enzymol. 31*, 667−678.
(15) Wohri, A. B., Wahlgren, W. Y., Malmerberg, E., Johansson, L. C., Neutze, R., and Katona, G. (2009) Lipidic sponge phase crystal structure of a photosynthetic reaction center reveals lipids on the protein surface. *Biochemistry 48*, 9831−9838.
(16) Michel, H. (1982) Three-dimensional crystals of a membrane protein complex. The photosynthetic reaction centre from *Rhodopseudomonas viridis*. *J. Mol. Biol. 158*, 567−572.
(17) Salom, D., Wu, N., Sun, W., Dong, Z., Palczewski, K., Jordan, S., and Salon, J. A. (2008) Heterologous expression and purification of the serotonin type 4 receptor from transgenic mouse retina. *Biochemistry 47*, 13296−13307.
(18) Kiser, P. D., Golczak, M., Lodowski, D. T., Chance, M. R., and Palczewski, K. (2009) Crystal structure of native RPE65, the retinoid isomerase of the visual cycle. *Proc. Natl. Acad. Sci. U.S.A. 106*, 17325−17330.
(19) Salom, D., Le Trong, I., Pohl, E., Ballesteros, J. A., Stenkamp, R. E., Palczewski, K., and Lodowski, D. T. (2006) Improvements in G protein-coupled receptor purification yield light stable rhodopsin crystals. *J. Struct. Biol. 156*, 497−504.
(20) Caffrey, M., and Cherezov, V. (2009) Crystallizing membrane proteins using lipidic mesophases. *Nat. Protoc. 4*, 706−731.
(21) Misquitta, Y., and Caffrey, M. (2003) Detergents destabilize the cubic phase of monoolein: Implications for membrane protein crystallization. *Biophys. J. 85*, 3084−3096.
(22) Fritzsch, G. (1998) Obtaining crystal structures from bacterial photosynthetic reaction centers. *Methods Enzymol. 297*, 57−77.
(23) Salom, D., Lodowski, D. T., Stenkamp, R. E., Le Trong, I., Golczak, M., Jastrzebska, B., Harris, T., Ballesteros, J. A., and Palczewski, K. (2006) Crystal structure of a photoactivated deprotonated intermediate of rhodopsin. *Proc. Natl. Acad. Sci. U.S.A. 103*, 16123−16128.
(24) Kovalevsky, A. Y., Hanson, B. L., Mason, S. A., Yoshida, T., Fisher, S. Z., Mustyakimov, M., Forsyth, V. T., Blakeley, M. P., Keen, D. A., and Langan, P. (2011) Identification of the Elusive Hydronium Ion Exchanging Roles with a Proton in an Enzyme at Lower pH Values. *Angew. Chem., Int. Ed. 50*, 7520−7523.
(25) Blake, C. C., Koenig, D. F., Mair, G. A., North, A. C., Phillips, D. C., and Sarma, V. R. (1965) Structure of hen egg-white lysozyme. A three-dimensional Fourier synthesis at 2 Å resolution. *Nature 206*, 757−761.
(26) Wang, J., Dauter, M., Alkire, R., Joachimiak, A., and Dauter, Z. (2007) Triclinic lysozyme at 0.65 Å resolution. *Acta Crystallogr. D63*, 1254−1268.
(27) Pompidor, G., Maury, O., Vicat, J., and Kahn, R. (2010) A dipicolinate lanthanide complex for solving protein structures using anomalous diffraction. *Acta Crystallogr. D66*, 762−769.
(28) Birdsall, D. L., and McPherson, A. (1992) Crystal structure disposition of thymidylic acid tetramer in complex with ribonuclease A. *J. Biol. Chem. 267*, 22230−22236.
(29) Tsina, E., Chen, C., Koutalos, Y., Ala-Laurila, P., Tsacopoulos, M., Wiggert, B., Crouch, R. K., and Cornwall, M. C. (2004) Physiological and microfluorometric studies of reduction and clearance of retinal in bleached rod photoreceptors. *J. Gen. Physiol. 124*, 429−443.
(30) Baxter, R. H., Ponomarenko, N., Srajer, V., Pahl, R., Moffat, K., and Norris, J. R. (2004) Time-resolved crystallographic studies of light-induced structural changes in the photosynthetic reaction center. *Proc. Natl. Acad. Sci. U.S.A. 101*, 5982−5987.
(31) Kochendoefer, G. G., and Mathies, R. A. (1996) Spontaneous emission study of the femtosecond isomerization dynamics of rhodopsin. *J. Phys. Chem. 100*, 14526−14532.
(32) Rieckhoff, K. E., and Peticolas, W. L. (1965) Optical Second-Harmonic Generation in Crystalline Amino Acids. *Science 147*, 610−611.
(33) Guptasarma, P. (2008) Solution-state characteristics of the ultraviolet A-induced visible fluorescence from proteins. *Arch. Biochem. Biophys. 478*, 127−129.
(34) Stadtman, E. R., and Levine, R. L. (2003) Free radical-mediated oxidation of free amino acids and amino acid residues in proteins. *Amino Acids 25*, 207−218.
(35) Boyland, E., Sims, P., and Williams, D. C. (1956) The oxidation of tryptophan and some related compounds with persulphate. *Biochem. J. 62*, 546−550.
(36) Gibson, E. A., Masihzadeh, O., Lei, T. C., Ammar, D. A., and Kahook, M. Y. (2011) Multiphoton microscopy for ophthalmic imaging. *J. Ophthalmol. 2011*, 870−879.
(37) Campagnola, P. (2011) Second harmonic generation imaging microscopy: Applications to diseases diagnostics. *Anal. Chem. 83*, 3224−3231.
(38) Ajeti, V., Nadiarnykh, O., Ponik, S. M., Keely, P. J., Eliceiri, K. W., and Campagnola, P. J. (2011) Structural changes in mixed Col I/Col V collagen gels probed by SHG microscopy: Implications for probing stromal alterations in human breast cancer. *Biomed. Opt. Express 2*, 2307−2316.
(39) Kissick, D. J., Wanapun, D., and Simpson, G. J. (2011) Second-order nonlinear optical imaging of chiral crystals. *Annu. Rev. Anal. Chem. 4*, 419−437.
(40) Moad, A. J., Moad, C. W., Perry, J. M., Wampler, R. D., Goeken, G. S., Begue, N. J., Shen, T., Heiland, R., and Simpson, G. J. (2007) NLOPredict: Visualization and data analysis software for nonlinear optics. *J. Comput. Chem. 28*, 1996−2002.

(41) Klapper, H., and Hahn, T. (2006) Point-group symmetry and physical properties of crystals. *Int. Tables X-Ray Crystallogr. A,*, 804–808.
(42) Stout, G. H., and Jensen, L. H. (1989) *X-ray structure determination: A practical guide*, 2nd ed., Wiley, New York.
(43) Shukla, A., Mukherjee, S., Sharma, S., Agrawal, V., Radha Kishan, K. V., and Guptasarma, P. (2004) A novel UV laser-induced visible blue radiation from protein crystals and aggregates: Scattering artifacts or fluorescence transitions of peptide electrons delocalized through hydrogen bonding? *Arch. Biochem. Biophys. 428*, 144–153.
(44) Del Mercato, L. L., Pompa, P. P., Maruccio, G., Della Torre, A., Sabella, S., Tamburro, A. M., Cingolani, R., and Rinaldi, R. (2007) Charge transport and intrinsic fluorescence in amyloid-like fibrils. *Proc. Natl. Acad. Sci. U.S.A. 104*, 18019–18024.
(45) Sharpe, S., Simonetti, K., Yau, J., and Walsh, P. (2011) Solid-State NMR characterization of autofluorescent fibrils formed by the elastin-derived peptide GVGVAGVG. *Biomacromolecules 12*, 1546–1555.
(46) Chu, C. C., and Imae, T. (2009) Fluorescence Investigations of Oxygen-Doped Simple Amine Compared with Fluorescent PAMAM Dendrimer. *Macromol. Rapid Commun. 30*, 89–93.
(47) Haupert, L. M., Simpson, G. J., and Slipchenko, L. V. (2011) Computational Investigation of Amine-Oxygen Exciplex Formation. *J. Phys. Chem. A 115*, 10159–10165.
(48) Bestvater, F., Spiess, E., Stobrawa, G., Hacker, M., Feurer, T., Porwol, T., Berchner-Pfannschmidt, U., Wotzlaw, C., and Acker, H. (2002) Two-photon fluorescence absorption and emission spectra of dyes relevant for cell imaging. *J. Microsc. (Oxford, U.K.) 208*, 108–115.
(49) Drobizhev, M., Makarov, N. S., Tillo, S. E., Hughes, T. E., and Rebane, A. (2011) Two-photon absorption properties of fluorescent proteins. *Nat. Methods 8*, 393–399.